Mon. Not. R. Astron. Soc. **000**, 1–12 (2009) Printed 18 January 2010 (MN LATEX style file v2.2)

Realistic Simulations of the Galactic Polarized Foreground: Consequences for 21-cm Reionization Detection Experiments

Vibor Jelić[1⋆], Saleem Zaroubi[1], Panagiotis Labropoulos[1], Gianni Bernardi[2], A. G. de Bruyn[1,3] and Léon V. E. Koopmans[1]
[1]*Kapteyn Astronomical Institute, University of Groningen, P.O. Box 800, 9700 AV Groningen, the Netherlands*
[2]*Harvard Smithsonian Center for Astrophysics, 60 Garden Street, Cambridge, MA 02138, USA*
[3]*ASTRON, P.O. Box 2, 7990 AA Dwingeloo, the Netherlands*

18 January 2010

ABSTRACT
Experiments designed to measure the redshifted 21 cm line from the Epoch of Reionization (EoR) are challenged by strong astrophysical foreground contamination, ionospheric distortions, complex instrumental response and other different types of noise (e.g. radio frequency interference). The astrophysical foregrounds are dominated by diffuse synchrotron emission from our Galaxy. Here we present a simulation of the Galactic emission used as a foreground module for the LOFAR- EoR key science project end-to-end simulations. The simulation produces total and polarized intensity over $10^\circ \times 10^\circ$ maps of the Galactic synchrotron and free-free emission, including all observed characteristics of the emission: spatial fluctuations of amplitude and spectral index of the synchrotron emission, together with Faraday rotation effects. The importance of these simulations arise from the fact that the Galactic polarized emission could behave in a manner similar to the EoR signal along the frequency direction. As a consequence, an improper instrumental calibration will give rise to leakages of the polarized to the total signal and mask the desired EoR signal. In this paper we address this for the first time through realistic simulations.

Key words: cosmology: theory, diffuse radiation, observation; radio lines: general; instrumentation: interferometers; radio continuum: general

1 INTRODUCTION

The Epoch of Reionization (EoR) is expected to occur between redshift 6 and 12, as indicated from observed comic microwave background (CMB) polarization (Komatsu et al. 2009) and high redshift quasar spectra (Fan et al. 2006). At redshifts, the 21 cm line from neutral hydrogen is shifted into meter wavelengths and therefore sets the frequency range of EoR experiments to the long-wavelength part of the radio spectrum ($\sim 100 - 200$ MHz).

There are several planned and ongoing experiments designed to probe the EoR through redshifted 21 cm emission line from neutral hydrogen using radio arrays: GMRT[1], LOFAR[2], MWA[3], 21CMA[4], PAPER[5], and SKA[6].

The low-frequency radio sky at these wavelengths is dominated by diffuse synchrotron emission from the Galaxy and integrated emission from extragalactic sources (radio galaxies and clusters). Although, this foreground emission is $4 - 5$ orders of magnitude stronger than the expected EoR signal, the ratio between their intensity fluctuations on arcmin to degree scales measured by interferometers is 'only' $2 - 3$ orders of magnitude (Shaver et al. 1999). In addition to the foregrounds, the EoR experiments are also challenged by understanding of the instrumental response and ionospheric disturbances to high precision (Labropoulos , in preparation).

Currently there are numerous efforts to simulate all the data components of the EoR experiments: cosmological 21 cm signal, foregrounds, ionosphere and instrumental response. The main aim of these end to end simulations is to develop a robust signal extraction scheme for the extremely challenging EoR observations (e.g. Santos et al. 2005; Morales et al. 2006; Wang et al. 2006; Jelić et al. 2008; Bowman et al. 2009; Harker et al. 2009a,b; Labropoulos et al. 2009).

The foregrounds in the context of the EoR measurements have been studied theoretically by various authors. Shaver et al. (1999) have given the first overview of the foreground components. Di Matteo et al. (2002, 2004) have studied emission from unresolved extragalactic sources at low radio frequencies. Oh & Mack (2003)

⋆ E-mail: vjelic@astro.rug.nl
[1] Giant Metrewave Telescope, http://gmrt.ncra.tifr.res.in
[2] Low Frequency Array, http://www.lofar.org
[3] Murchinson Widefield Array, http://www.mwatelescope.org/
[4] 21 Centimeter Array, http://21cma.bao.ac.cn/
[5] Precision Array to Probe EoR, http://astro.berkeley.edu/~dbacker/eor
[6] Square Kilometer Array, http://www.skatelescope.org/

and Cooray (2004) have considered the effect of free-free emission from extragalactic haloes. Santos et al. (2005) carried out a detailed study of the functional form of the foreground correlations. Jelić et al. (2008) have made the first detailed foreground model and have simulated the maps that include both the diffuse emission from our Galaxy and extragalactic sources (radio galaxies and clusters). Gleser et al. (2008) have also studied both galactic and extragalactic foregrounds. de Oliveira-Costa et al. (2008) has used all publicly available total power radio surveys to obtain all-sky Galactic maps at the desired frequency range and Bowman et al. (2009) has studied foreground contamination in the context of the power spectrum estimation.

Recently, a Galactic 3D emission model has been developed by Sun et al. (2008); Waelkens et al. (2009); Sun & Reich (2009) (the HAMMURABI[7] code), derived from a 3D distribution of the Galactic thermal electrons, cosmic-ray electrons and magnetic fields. The code is able to reproduce all-sky or zoom-in maps of the Galactic emission over a wide frequency range.

In addition to simulations, a number of observational projects have given estimates of Galactic foregrounds in small selected areas. Ali et al. (2008) have used 153 MHz observations with GMRT to characterize the visibility correlation function of the foregrounds. Rogers & Bowman (2008) have measured the spectral index of the diffuse radio background between 100 and 200 MHz. Pen et al. (2009) has set an upper limit to the diffuse polarized Galactic emission; and Bernardi et al. (2009, and submitted) obtained the most recent and comprehensive targeted observations with the Westerbork Synthesis Radio Telescope (WSRT).

However, current observations are not able to fully constrain the foregrounds, especial the Galactic polarized synchrotron emission, as required by EoR experiments. The importance of the polarized foreground stems from the fact that the LOFAR instrument, in common with all current interferometric EoR experiments, has an instrumentally polarized response. An improper polarization calibration will give rise to leakages of the complex polarized signal to the total signal. Since the Galactic polarized emission is quite structured along the frequency direction, the leakage of polarized intensity will have similar structures along the frequency and will mimic the EoR signal. Therefore, for reliable detection of the EoR signal it is essential at this stage, to simulate the polarized foregrounds, the instrumental response and test the influence of the leakages on the extraction of the EoR signal.

In our previous model (Jelić et al. 2008), the total intensity Galactic emission maps were obtained from three Gaussian random fields. The first two were for the amplitudes of synchrotron and free-free emission and the third was for the spectral index of the synchrotron emission. The polarized maps were simulated in a similar way but with added multiple 2D Faraday screens along the line of sight. Despite the ability of that model to simulate observed characteristics of the Galactic emission (e.g. spatial and frequency variations of brightness temperature and its spectral index), the model had some disadvantages: e.g. the Galactic emission was derived *ad hoc* and depolarization effects were not taken into account.

This paper focuses on simulating the Galactic synchrotron and free-free emission in total and polarized intensity, as an extension of our previous foreground model (Jelić et al. 2008) for the LOFAR-EoR experiment. The Galactic emission in our current model is derived from the physical quantities and 3D characteristics of the Galaxy (e.g. the cosmic ray and thermal electron density, and the magnetic field). In addition, the model has the flexibility to simulate any peculiar case of the Galactic emission including very complex polarized structures produced by"Faraday screens" and depolarization due to Faraday thick layers.

Our Galactic emission model has some similarities with the HAMMURABI model, but the difference between the two is the main purpose of the simulations. The HAMMURABI simulation is based on a very complex Galactic model with aim to reproduce the observed all-sky maps of the Galactic emission. Because of its complexity, the high resolution zoom-in maps require a lot of computing power and time (Sun & Reich 2009). In contrast, our model is restricted to produce fast and relatively small maps of Galactic emission, which are then used as a foreground template for the LOFAR-EoR end to end simulation. Since the foreground subtraction is usually done along the frequency direction, our simple model also includes 3D spatial variations of the spectral index of the Galactic synchrotron radiation.

The paper is organized as follows. Section 2 gives a brief theoretical overview of the Galactic emission and Faraday rotation. The observational constrains of the Galactic emission are presented in Sec. 3. The simulation algorithm is described in Sec. 4, while a few simulated maps for peculiar cases of the Galactic emission are presented in Sec. 5. Section 6 describes the LOFAR-EoR pipeline. We illustrate the need for a good polarization calibration in Sec. 7. The paper concludes with summary and outlook (Sec. 8).

2 THEORY

In radio astronomy, at frequencies where the Rayleigh-Jeans law is applicable, the radiation intensity, I (energy emitted per unit time per solid angle and per unit area and unit frequency), at the frequency ν is commonly expressed in terms of the brightness temperature (T_b):

$$T_b(\nu) = \frac{c^2}{2k_B\nu^2} I(\nu), \tag{1}$$

where c is the speed of light and k_B Boltzmann's constant.

The emission coefficient, j (energy emitted per unit time per solid angle and per unit volume), at a certain frequency can also be expressed in terms of the unit temperature, $j_b(\nu) = \frac{c^2}{2k_B\nu^2} j(\nu)$, so that:

$$T_b(\nu) = \int j_b(\nu) \mathrm{d}s, \tag{2}$$

where the integral is taken along the line of sight (LOS).

In the following subsection we will give a brief theoretical overview of the Galactic synchrotron and free-free emission, as well as Faraday rotation, that will be used later in the simulation. The Galactic emission will be expressed in terms of j_b and T_b.

2.1 Synchrotron emission

Synchrotron emission originates from the interaction between relativistically moving charges and magnetic fields. In our own galaxy, synchrotron emission arises from cosmic ray (CR) electrons produced mostly by supernova explosions and the Galactic magnetic field. A fairly complete exposition of the synchrotron emission theory is presented in e.g. Pacholczyk (1970) and Rybicki & Lightman (1986). Here we only give a simple description of the emission.

The Galactic synchrotron emission (GSE) is partially linearly

[7] http://www.mpa-garching.mpg.de/hammurabi/

polarized. Its properties depend on the spatial and energy distribution of the CR electrons, and the strength and orientation of the perpendicular (with respect to the LOS) component of the Galactic magnetic field, $B_\perp$. The emission coefficients of the Galactic total and polarized synchrotron radiation, j_b^{Isyn} and j_b^{PIsyn}, are given respectively in cgs units, at the frequency ν, by:

$$j_b^{I,PIsyn} = C_{I,PIsyn} \left(\frac{2\pi m_e c}{3e}\right)^{-\frac{p-1}{2}} n_{\rm CR} B_\perp^{\frac{p+1}{2}} \nu^{-\frac{p+3}{2}}, \quad (3)$$

with

$$C_{Isyn} = \frac{\sqrt{3}e^3}{8\pi m_e k_B (p+1)} \Gamma\left(\frac{p}{4} - \frac{1}{12}\right) \Gamma\left(\frac{p}{4} + \frac{19}{12}\right), \quad (4)$$

$$C_{PIsyn} = \frac{\sqrt{3}e^3}{32\pi m_e k_B} \Gamma\left(\frac{p}{4} - \frac{1}{12}\right) \Gamma\left(\frac{p}{4} + \frac{7}{12}\right). \quad (5)$$

The charge of the electron is given by $e = 4.8 \cdot 10^{-10}$ Fr, the mass by $m_e = 9.1 \cdot 10^{-28}$ g and $n_{\rm CR}$ is the CR electron density. Note that for the CR electrons we assume that their energy spectrum is a power law with a spectral index p: $N(\gamma)\mathrm{d}\gamma = n_{\rm CR0}\gamma^{-p}$, where γ is the Lorenz factor and $N(\gamma)$ the number density of electrons with energy between γ and $\gamma + \mathrm{d}\gamma$ and $n_{\rm CR0}$ normalization constant. Furthermore, we assume that their velocity and pitch angle distribution is isotropic. Both simplifications are consistent with observations and are widely used by many authors (e.g. Sun et al. 2008; Waelkens et al. 2009, as most recent examples). Note that the intrinsic degree of polarization of synchrotron radiation depends on the energy spectral index p and is given by

$$\Pi = \frac{p+1}{p+7/3}. \quad (6)$$

The Stokes Q and U parameters of the polarized GSE are given by:

$$j_b^Q = j_b^{PIsyn} \cos 2\Phi, \quad (7)$$

$$j_b^U = j_b^{PIsyn} \sin 2\Phi, \quad (8)$$

where Φ is polarization angle defined with respect to the orientation of the magnetic field.

By integrating j_b^{Isyn}, j_b^Q & j_b^U along some LOS (see Eq. 2) we get the total and polarized Galactic synchrotron emission in terms of the brightness temperature (T_b^{Isyn}, T_b^Q & T_b^U). Note that observed polarized emission and polarization angle Φ_{obs} are given by:

$$T_b^{PI} = \sqrt{(T_b^Q)^2 + (T_b^U)^2}, \quad (9)$$

$$\Phi_{obs} = \frac{1}{2} \arctan \frac{T_b^U}{T_b^Q}. \quad (10)$$

2.2 Free-free emission

Radiation due to (de)acceleration of a charged particle in the electrical field of another is called bremsstrahlung or free-free radiation. The Galactic free-free emission originates from electron-ion encounter in the warm ionized gas. As for the synchrotron emission a detail theory of the free-free radiation can be found in e.g. Rybicki & Lightman (1986) and Wilson et al. (2009), here we give only the necessary formulae.

The optical depth, τ_ν^{ff}, of the warm ionized gas at a given low radio frequency ν is:

$$\tau_\nu^{ff} = 3.01 \cdot 10^{-8} g_{ff} \left(\frac{T_e}{[\mathrm{K}]}\right)^{-\frac{3}{2}} \left(\frac{\nu}{[\mathrm{MHz}]}\right)^{-2} \frac{EM}{[\mathrm{cm}^{-6}\mathrm{pc}]}, \quad (11)$$

where T_e is temperature of the ionized gas, g_{ff} is the Gaunt factor of the free-free transition given by:

$$g_{ff} = \ln\left[4.95 \cdot 10^{-5} \left(\frac{\nu}{[\mathrm{MHz}]}\right)^{-1}\right] + 1.5 \ln\left(\frac{T_e}{[\mathrm{K}]}\right), \quad (12)$$

and EM is emission measure defined as:

$$\frac{EM}{[\mathrm{cm}^{-6}\mathrm{pc}]} = \int n_e^2 \mathrm{d}s. \quad (13)$$

The integral is taken over the LOS, where n_e in cm^{-3} is the electron density of the warm ionized gas.

The Galactic free-free emission in terms of brightness temperature, j_b^{ff}, is given by:

$$j_b^{ff} = T_e(1 - \mathrm{e}^{-\tau^{ff}}). \quad (14)$$

Note that for optically thin ionized gas, j_b^{ff} is simply given by $j_b^{ff} = T_e \tau^{ff}$.

2.3 Faraday rotation

When the polarization angle of an electromagnetic wave is rotated while passing through a magnetized plasma, the effect is called Faraday rotation (for details see Rybicki & Lightman 1986; Wilson et al. 2009). The rotation depends on the frequency of the wave, ν, electron density, n_e, and magnetic field component parallel to the LOS, $B_\parallel$:

$$\Phi = \Phi_0 + \frac{e^3}{2\pi m_e^2 c^2} \nu^{-2} \int n_e B_\parallel \mathrm{d}s, \quad (15)$$

where the polarization angle of the wave before rotation is denoted with Φ_0. Eq. 15 is also written as $\Phi = \Phi_0 + RM\lambda^2$ with λ in units of m and RM (rotation measure) defined as:

$$\frac{RM}{[\mathrm{rad\ m}^{-2}]} = 0.81 \int \frac{n_e}{[\mathrm{cm}^{-3}]} \frac{B_\parallel}{[\mu\mathrm{G}]} \frac{\mathrm{d}s}{[\mathrm{pc}]}. \quad (16)$$

The RM is positive when $B_\parallel$ points towards observer and negative when $B_\parallel$ points in away.

3 OBSERVATIONAL CONSTRAINTS

There are several all-sky maps of the total Galactic diffuse radio emission at different frequencies and angular resolutions (Haslam et al. 1982; Reich & Reich 1986, 1988; Page et al. 2007). The 150 MHz map by Landecker & Wielebinski (1970) is the only all-sky map in the frequency range ($100 - 200$ MHz) relevant for the EoR experiments, but has only 5° resolution.

At high Galactic latitudes the minimum brightness temperature of the Galactic diffuse emission is about 20 K at 325 MHz with variations of the order of 2 per cent on scales from 5 to 30 arcmin across the sky (de Bruyn et al. 1998). At the same Galactic latitudes, the temperature spectral index of the Galactic emission is about -2.55 at between 100 and 200 MHz (Rogers & Bowman 2008) and steepens towards higher frequencies (e.g. Platania et al. 1998; Bennett et al. 2003; Bernardi et al. 2004). Furthermore, the spectral index gradually changes with position on the sky. This change appears to be caused by a variation in the spectral index along the line of sight. An appropriate standard deviation in the

power law index, in the frequency range 100–200 MHz appears to be of the order of ~ 0.1 (Shaver et al. 1999).

Using the obtained values at 325 MHz and assuming the frequency power law dependence, the Galactic diffuse emission is expected to be 140 K at 150 MHz, with ~ 3 K fluctuations.

Studies of the Galactic polarized diffuse emission are done mostly at high radio ($\sim$ 1GHz) frequencies (for a recent review see, Reich 2006). At lower frequencies (~ 350 MHz), there are several fields done with the Westerbork telescope (WSRT) (Wieringa et al. 1993; Haverkorn et al. 2003; Schnitzler 2008). These studies revealed a large number of unusually shaped polarized small-scale structures of the Galactic emission, which have no counterpart in the total intensity. These structures are usually attributed to the Faraday rotation effects along the line of sight. A recent method by Brentjens & de Bruyn (2005, Faraday rotation measure synthesis) allows to overcome the problem of bandwidth depolarization and to distinguish among different synchrotron emitting regions along the line of sight.

At high Galactic latitudes, the Galactic polarized emission at 350 MHz is around 5 K or more, on 5–10 arcmin scales (de Bruyn et al. 2006). At 150 MHz this polarized emission would scale to few tens of Kelvin if it were Faraday thin. However, depolarization, that is prominent at low radio frequencies, can significantly lower the level of polarized emission.

Recently, a comprehensive program was initiated by the LOFAR-EoR collaboration to directly measure the properties of the Galactic radio emission in the frequency range relevant for the EoR experiments. The observations were carried out using the Low Frequency Front Ends (LFFE) on the WSRT radio telescope. Three different fields were observed. The first field was a highly polarized region known as the "Fan region" in the 2nd Galactic quadrant at a low Galactic latitude of $\sim 10^\circ$ Bernardi et al. (2009). The second field was a very cold region in the Galactic halo ($l \sim 170^\circ$) around the bright radio quasar 3C196, and third was a region around the North Celestial Pole (NCP, $l \sim 125^\circ$, Bernardi et al., *submitted*). The last two fields represent possible targets for the LOFAR-EoR observations. Below we present the main results of these papers.

In the "Fan region", fluctuations of the Galactic diffuse emission were detected at 150 MHz for the first time. The fluctuations were detected both in total and polarized intensity, with an rms of 14 K (13 arcmin resolution) and 7.2 K (4 arcmin resolution) respectively (Bernardi et al. 2009). Their spatial structure appeared to have a power law behavior with a slope of -2.2 ± 0.3 in total intensity and -1.65 ± 0.15 in polarized intensity. Note that, due to its strong polarized emission, the "Fan region" is not a representative part of the high Galactic latitude sky.

Fluctuations of the total intensity Galactic diffuse emission in the "3C196" and "NGP" fields were also observed on scales larger than 30 arcmin, with an rms of 3.3 K and 5.5 K respectively.

Patchy polarized emission was found in the "3C196" field, with an rms value of 0.68 K on scales larger than 30 arcmin (Bernardi et al., *submitted*). Thus, the Galactic polarized emission fluctuations seem to be smaller than expected by extrapolating from higher frequency observations. Recent observations at mid-galactic latitude with the Giant Metrewave Radio Telescope (GMRT) confirm this conclusion, by setting an upper limit to the diffuse polarized Galactic emission in their field to be < 3 K at 150 MHz and on scales between 36 and 10 arcmin (Pen et al. 2009).

4 SIMULATION

In this section, the various components of the simulation that lead towards the brightness temperature maps of the Galactic synchrotron and free-free emission in a total and polarized intensity are explained. Because the simulated maps will be used as a foreground template for the LOFAR-EoR end-to-end simulations, the foreground simulations assume the angular and frequency range of the LOFAR-EoR experiment, i.e. $10^\circ \times 10^\circ$ maps from 115 MHz to 180 MHz. In addition, all parameters of the simulations can be tuned to any desired value or have any desired characteristic, allowing to explore the parameter space of our Galactic model.

The first step in our simulation is to calculate, at a certain frequency, the 3D emission coefficient of the Galactic synchrotron and free-free emission expressed in terms of unit temperature (see Eq. 3 & 14). The emission coefficients are obtained from the cosmic-ray, $n_{\rm CR}$, and thermal electron, n_e, densities, and the Galactic magnetic field ($\vec{B}$). Given the 3D emission coefficients, we integrate along the LOS to obtain the brightness temperature maps of the Galactic synchrotron and free-free emission at a certain frequency. The calculation also includes Faraday rotation effects. Note that all parameters of the simulation are set to be in an agreement with the observed properties of the Galactic emission.

Our algorithm is based on a 3D grid in a Cartesian coordinate system, where xy-plane represents the angular plane of the sky ("flat sky" approximation valid for a small field of view) and z axis is a line of sight direction in parsecs.

In the following subsections we describe in detail the inputs ($n_{\rm CR}$, n_e and $\vec{B}$) and the algorithm that is used to obtain the Galactic emission maps. The simulated maps of a few different cases of the Galactic emission will be presented in Sec. 5.

4.1 Cosmic ray electron density

The cosmic ray (CR) electrons relevant for the Galactic synchrotron emission have energies between 400 MeV and 25 GeV, assuming a Galactic magnetic field of a few μG (Webber et al. 1980). In this energy range, the CR electron distribution can be described as a power law. The power law is normalized according to the measurements obtained in the solar neighborhood. However, the locally measured values might not be a good representative for the CR density elsewhere in the Galaxy (e.g. Strong et al. 2004). As a consequence, the CR electron distribution is weakly constrained.

In our simulation, uniform CR electron density distribution is assumed in the xy-plane. In the z direction we follow Sun et al. (2008) and assume an exponential distribution:

$$n_{\rm CR} = n_{\rm CR0} \exp\left(\frac{-z}{1\rm kpc}\right). \quad (17)$$

Note that $n_{\rm CR0}$ depends on the assumed energy spectral index p of the CR electrons, so it is normalized according to Eq. 2 for the synchrotron radiation. Assuming $T_b(150\ \rm MHz) \simeq 145$ K, $B_\perp = 5\ \mu$G and $p = 2$, we get $n_{\rm CR0} \simeq 1.4 \cdot 10^{-8}\ \rm cm^{-3}$.

In the desired frequency range of our simulation, the assumed energy spectral index $p = 2$ is consistent with the values of the typically observed brightness temperature spectral index of the Galactic synchrotron emission ($\beta = -2.5$, see Sec. 3)[8].

[8] The brightness temperature spectral index β of the Galactic synchrotron emission and the energy spectral index p of the CR electrons are related as $\beta = -(p+3)/2$.

In addition, the spatial variations of the spectral index p are introduced to mimic the observed spatial fluctuations of β. We follow our previous model (Jelić et al. 2008) and simulate the variation of p (or β) as a Gaussian random field (GRF). For the power spectrum of the GRF it is assumed a power law with index -2.7 (Jelić et al. 2008).

4.2 Galactic magnetic field

The Galactic magnetic field has two components: a regular component $\vec{B_r}$ and a random component $\vec{b}$, so that the total Galactic magnetic field is given as $\vec{B} = \vec{B_r} + \vec{b}$ (for review see Beck et al. 1996; Han & Wielebinski 2002). The regular component is usually simulated as a combination of a disk and a halo field, whereas the random field component is simulated as a Gaussian random field, GRF, (for details see Sun et al. 2008; Sun & Reich 2009). Note that for our calculations, we split $\vec{B}$ in a component parallel ($B_\parallel$) and perpendicular ($B_\perp$) to the LOS, so that Faraday rotation is defined by $B_\parallel$ and synchrotron emission by $B_\perp$.

Considering the aim of our effort to simulate the Galactic emission for a small patch of the sky, we treat the regular field component in a simplified way. The regular field component is assumed to be uniform in the xy-plane and to have an exponential decrease in the z direction. The typical value of the regular field component is a few μG (for review see Beck et al. 1996; Han & Wielebinski 2002).

For the random field component we follow Sun et al. (2008); Sun & Reich (2009) and simulate it as a GRF. The power spectrum of the field follows a power law, with spectral index $-8/3$. This spectral index is commonly used for a Kolmogorov-like turbulence spectrum.

In our simulation, the realization of the random field component is done in the following way. First we generate three different GRFs for the b_x, b_y and b_z component. From those three fields, we then calculate the amplitude of $\vec{b}$ and normalize it to the desired value. A typical value for the mean random field strength is $b = 3\ \mu$G (Sun et al. 2008).

4.3 Thermal electron density

At high Galactic latitudes, the warm ionized medium consists mostly of diffuse ionized gas (DIG) with total emission measure of $\sim 5\ \mathrm{pc\ cm^{-6}}$ and $T_e = 8000$ K (Reynolds 1990). The properties of the DIG can be traced by its free-free emission and dispersion measure[9] (DM) of pulsars (e.g. Gaensler et al. 2008).

Recent simulations of the Galactic emission (Sun et al. 2008; Waelkens et al. 2009; Sun & Reich 2009) used the Cordes & Lazio (2002) model for the thermal electron distribution. That model simulates the Galaxy as several large-scale (e.g. thin and thick disk, and spiral arms) and small-scale (e.g. supernovae bubbles) structures. In our simulation, we follow our previous model of the Galactic free-free emission (Jelić et al. 2008) and simulate the thermal electron density distribution as a GRF with the power law type of the spectrum. The spectral index of the power law is -3. The amplitude of the GRF (thermal electron density) is normalized in a way to match the typical observed EM of the quasars at high Galactic latitudes (EM values are taken from Berkhuijsen et al. 2006).

It is important to note that our model is flexible to include additional features of the thermal electron distribution, e.g. dense bubbles or clumpy distribution. Some of these features are presented in Sec. 5.

[9] The dispersion measure is defined as the integral of the thermal electron density along the LOS. Knowing the distance to the pulsars (e.g. determined by parallax), an electron density model can be obtained by a fit to the observed DMs.

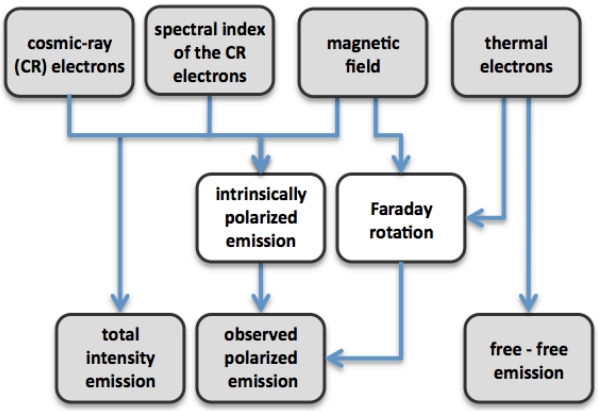

Figure 1. Flow chart of the algorithm: the Galactic emission (synchrotron and free- free) is derived from the physical quantities and 3D characteristics of the Galaxy, i.e. cosmic ray, n_{CR}, and thermal electron, n_e, density; and magnetic field, $\vec{B}$. In addition, the algorithm includes Faraday rotation effects.

4.4 The Algorithm

Here we summarize the steps we follow to obtain maps of the Galactic emission at a desired frequency. The flow chart of the algorithm is presented in Fig. 1.

(i) The CR electron density, n_{CR}, and the regular component, $\vec{B_r}$, of the Galactic magnetic field are defined on 3D grid. The distributions of n_{CR} and $\vec{B_r}$ are uniform in the xy-plane and have an exponential decrease in the z direction.

(ii) The spatial distribution of the CR electron energy spectral index, p, the random component, $\vec{b}$, of the Galactic magnetic field and the thermal electron density, n_e, are simulated as GRFs. The GRFs are normalized to result in a desired rms value of the brightness temperature maps. Note that additional features in the electron distribution are added if desired.

(iii) The parallel, $B_\parallel$, and perpendicular, $B_\perp$, component of the total Galactic magnetic field, $\vec{B}$, are calculated from $\vec{B_r}$ and $\vec{b}$.

(iv) Using Eq. 3, the emission coefficients of the Galactic total, j_b^{Isyn}, and polarized, j_b^{PIsyn}, synchrotron radiation are calculated.

(v) The optical depth, τ^{ff}, and emission coefficient, j_b^{ff}, of the thermal plasma are obtained from Eq. 11 & 14. Note that these effect is really significant only on the lowest radio frequencies.

(vi) Absorption of the synchrotron emission by the optical thickness of the ionized plasma is taken into account as $\exp(-\tau^{ff})$ factor.

(vii) Using Eq. 15, the Faraday rotation effect is calculated and the polarization angle, Φ, is obtained. Note that the intrinsic polarization angle, Φ_0, is defined as the inclination of $B_\perp$.

(viii) The Stokes Q and U emission coefficients of the polarized emission, j_b^Q & j_b^U, are calculated using Eq. 7 & 8.

(ix) By integrating j_b^{Isyn}, j_b^Q & j_b^U along some LOS (see Eq. 2), the total and polarized Galactic synchrotron emission in terms of the brightness temperature, T_b^{Isyn}, T_b^Q & T_b^U, are obtained.

Table 1. The physical parameters of CR electrons, thermal electrons and magnetic field used to calculate the Galactic emission. The same values are used in all four models.

$\bar{p}$	$n_{\rm CR0}$ [$\rm cm^{-3}$]	$B_{r,\parallel}$ [μG]	$B_{r,\perp}$ [μG]	$E\bar{M}$ [$\rm cm^{-6}pc$]	T_e [K]
2	$1.4 \cdot 10^{-8}$	3	2.5	8	8000

(x) Finally, the maps of the total polarized emission (T_b^{PI}) and observed polarization angle Φ_{obs} is calculated using Eq. 9 & 10.

In the following section we will show some examples of the Galactic emission maps obtained by this algorithm.

5 EXAMPLES

Here we demonstrate the ability of our algorithm to simulate synchrotron and free-free maps both in total and polarized intensity for different examples of the spatial distribution of Galactic emission. The maps are presented for four simple Galactic emission models, each with their own peculiarity:

- Model A: CR electrons are distributed in a region of 1 kpc in depth along the LOS. In front of this region, there is a thermal electron cloud of 300 pc in depth along the LOS. The thermal electron cloud is acting as a "Faraday screen" that rotates the polarization angle of synchrotron emission. The intensity of the polarized emission is unchanged.
- Model B: Both CR and thermal electrons are mixed in the region of 1 kpc in depth along the LOS. The polarized synchrotron radiation is differentially Faraday rotated and depolarization occurs.
- Model C: CR electrons are distributed in the same way as in the MODEL A, while the thermal electrons are mixed in the first and the last one-third of the CR electron region. The middle region, with only CR electrons, will enhance the coherence in polarized emission.
- Model D: The same as model B, but in the middle of the simulated region there is a dense thermal electron bubble 300 pc in depth along the LOS, with a strong magnetic field $B_{\parallel} = 10$ μG. The Faraday rotation along the bubble will be much larger than in other parts of the region. Note that the size of the bubble is quite larger in order to make its appearance in the final maps more clear.

Note that for simplicity we ignore the random component of the Galactic magnetic field. As a consequence, depolarization is produced only by thermal plasma.

In reality, the Galactic emission is much more complicated than these examples suggest. Therefore, in the LOFAR-EoR end-to-end simulations we use a combination of these simple models as our Galactic foreground template. In this paper, our goal is to test the functionality of the simulations.

The physical parameters used to calculate Galactic emission are presented in Table 1. The maps are obtained in the frequency range from 115 to 180 MHz, with 0.5 MHz step.

The synchrotron emission originates from the same CR electron distribution in all four models. Therefore, the brightness temperature maps of the total and intrinsic[10] polarized synchrotron emission are equivalent in all four models. The same is valid for the free-free emission, i.e., n_e is normalized to the same value of EM. The resulting $10^\circ \times 10^\circ$ maps at 150 MHz are shown in Fig. 3, while the $mean$ and rms of the maps are given in Table 2.

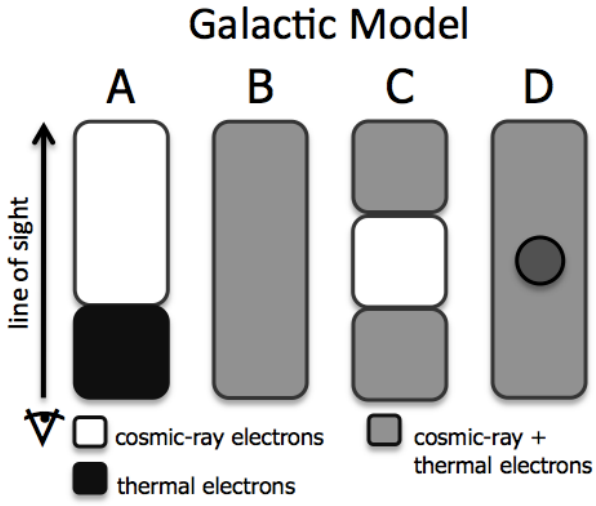

Figure 2. The intensity distributions (see Fig. 3 & 4) are obtained for four different models of the Galactic emission . The first (model A) assumes that synchrotron and free-free emitters are spatially separated, so that thermal plasma acts as a "Faraday screen". The second, third and fourth (model B, C, & D) have regions where both types permeate in a different way. The synchrotron emission is differentially Faraday rotated and depolarization occurs.

Table 2. The $mean$ and rms value of the maps shown in the Fig. 3 & 4. All the values are given in kelvin. For completeness, degree of polarized (PI/T) and depolarized ($dep.$) emission is calculated.

	I_{syn}	I_{ff}	iPI_{syn}	PI_A	PI_B	PI_C	PI_D
mean	142	1.5	98	98	10	34	11
rms	3	0.1	2	2	5	15	5
PI/I	-	-	69%	69%	7%	23%	8%
$dep.$	-	-	0%	0%	90%	66%	88%

As a first test of our algorithm, we estimate the degree of intrinsic polarization, Π, from the simulated maps. By dividing the intrinsic polarized emission map and the total intensity map, we obtain $\Pi = 0.69$ (see Table 2). This value is in a good agreement with the expected theoretical value $\Pi_{p=2} = 9/13$ (see Eq. 6).

The second test is to estimate the brightness temperature spectral index, β_{syn}, of the Galactic synchrotron emission. The index β_{syn} is estimated from the frequency data cube (i.e., maps of the emission as a function of frequency). The obtained map of β_{syn} is shown in the Fig. 3 (*third panel*). The $mean$ value of β_{syn} is -2.50, which is in a good agreement with the expected theoretical value $\beta_{p=2} = -(p+3)/2 = -2.55$. A slight difference between the two is caused by the 3D spatial variations of the spectral index p. Recall that variations of β_{syn} are important for testing the foreground subtraction algorithms.

Simulated polarized emission maps of the four Galactic synchrotron emission models are shown in Fig. 4. Their $mean$ and

[10] Here, the intrinsic polarized emission, $iPI_{\rm syn}$, means emission defined by Eq. 3. Note that the polarization angle of this emission is assumed to be uniform across the whole region. Thus any effect caused by thermal electrons will be immediately apparent.

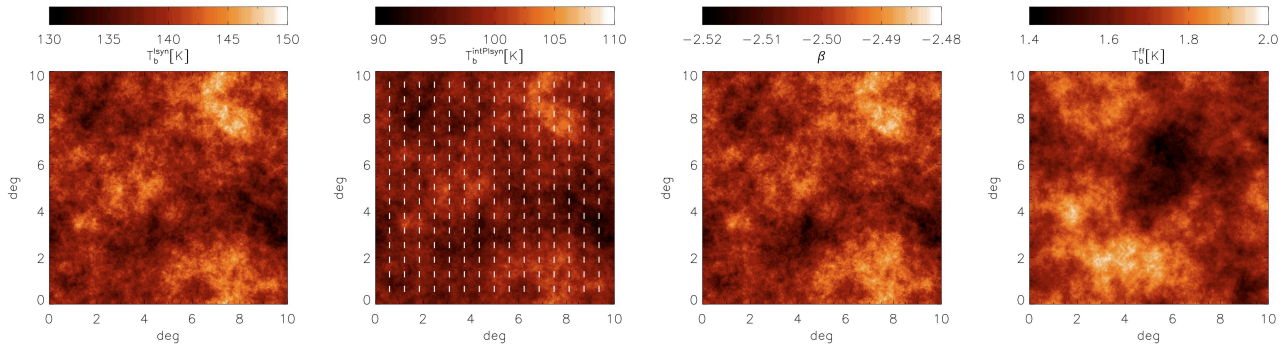

Figure 3. Simulated maps of the total (*first panel*) and intrinsic polarized (*second panel*) intensity of the Galactic synchrotron emission. The polarization angle is plotted over the polarized map as a white lines. The map of brightness temperature spectral index β of simulated total intensity synchrotron emission is shown on the *third panel*. The total intensity map of the free-free emission is shown on the *fourth panel*. The angular size of the maps are $10^\circ \times 10^\circ$, with ~ 1 arcmin resolution. The color bar represents the brightness temperature T_b of emission in kelvin at 150 MHz. The $mean$ and rms value of the maps are given in the Table 2.

rms values together with the degree of polarization and depolarization are listed in Table 2. Comparing the intrinsically polarized emission (*second panel* in the Fig. 3) with the polarized emission in the four models (see Fig. 4), we conclude that all maps have the characteristics as expected.

Model A assumes that there is no region in which the plasma (thermal electron cloud) is mixed with CR electrons. Therefore, polarization angles along the LOS are Faraday rotated by an equal anglethe (defined by Eq. 15). Since there is no differential Faraday rotation, the polarized intensity of the synchrotron emission is unchanged (see *first panel* on the Fig. 4). Note that fluctuations of the polarization angle over the map are determined only by the spatial RM fluctuations of the plasma.

In B, C and D models there are regions where both CR and thermal electrons are mixed. The polarization angle of the synchrotron radiation is then differentially Faraday rotated along the LOS in those regions. As a result, the polarized synchrotron radiation is quenched. The level of the polarized emission is smaller than intrinsic polarization emission. Note that the depolarization is smaller in model C than in B and D, since in the former there is a region with only synchrotron emission.

In Fig. 5, we show a random sight line along the frequency direction through synchrotron total intensity, I_{syn}, and polarized intensity, PI_{syn} data cubes. We also show a line of sight in Stokes, Q_{syn}. The lines are presented for models A, B, and D in the Fig. 5 (solid, dashed and dotted line).

The lines through the total intensity data cubes are obviously the same in all three models. The lines are smooth functions along the frequency direction and are the result of the superposition of power laws. The lines in polarized intensity are quite different. Models B and D show the fluctuations along the frequency direction, while model A shows a power law behavior as in total intensity. The fluctuations along the frequency direction are produced by the regions where both CR and thermal electrons are embedded together. The synchrotron radiation along the line of sight is not uniformly Faraday rotated and depolarization occurs. Since the model D has a region with high density plasma and strong magnetic field, differential Faraday rotation is more prominent than in model B and the fluctuations show more structures. Model A shows no fluctuations, since the whole synchrotron emission is uniformly Faraday rotated along the line of sight and depolarization does not occur.

In the Sec. 7, we explore leakages of the polarized structures to the total intensity data caused by an improper polarization calibration of the LOFAR telescope. Full understanding of these leakages is necessary in all EoR experiments, because they could contaminate the EoR signal.

6 LOFAR-EOR SIMULATION PIPELINE

The LOFAR-EoR project relies on a detailed understanding of astrophysical and non-astrophysical contaminations that can contaminate the EoR signal: the Galactic and extragalactic foregrounds, ionosphere, instrumental effects and systematics. In order to study these components and their influence on the detection of the EoR signal, a LOFAR-EoR simulation pipeline is being developed by the LOFAR-EoR team. The pipeline consists of the three main modules: the EoR signal (based on simulations described in Thomas et al. 2009), the foregrounds (based on this paper and Jelić et al. 2008) and the instrumental response (described on Labropoulos et al. 2009).

In this paper we use the LOFAR-EoR pipeline to illustrate the need for excellent calibration of the instrument in order to reliably detect the EoR signal (see Sec. 7). The following two subsections present a brief overview of the EoR signal and instrumental response modules.

6.1 EoR signal

The predicted differential brightness temperature of the cosmological 21 cm signal with the CMB as the background is given by (Field 1958, 1959; Ciardi & Madau 2003):

$$\delta T_{\rm b} = 26\ {\rm mK}\ x_{\rm HI}(1+\delta)\left(1-\frac{T_{\rm CMB}}{T_{\rm s}}\right)\left(\frac{\Omega_{\rm b}h^2}{0.02}\right)\left[\left(\frac{1+z}{10}\right)\left(\frac{0.3}{\Omega_{\rm m}}\right)\right]^{1/2}. \quad (18)$$

Here $T_{\rm s}$ is the spin temperature, $x_{\rm HI}$ is the neutral hydrogen fraction, δ is the matter density contrast and $h = H_0/(100\ {\rm km\ s^{-1}Mpc^{-1}})$. Throughout we assume ΛCDM-cosmology with WMAP3 parameters (Spergel et al. 2007): $h = 0.73$, $\Omega_{\rm b} = 0.0418$, $\Omega_{\rm m} = 0.238$ and $\Omega_\Lambda = 0.762$. In addition we

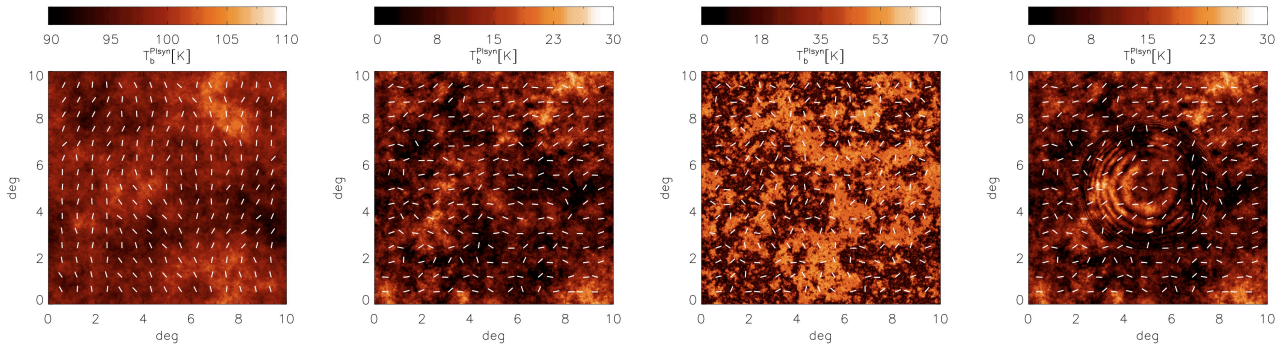

Figure 4. Simulated maps of the polarized intensity and polarization angle (white lines) of the four different Galactic synchrotron emission models (A, B, C and D from left to right). The angular size of the maps are $10^\circ \times 10^\circ$, with ~ 1 arcmin resolution. The $mean$ and rms values of the maps at 150 MHz are given in the Table 2.

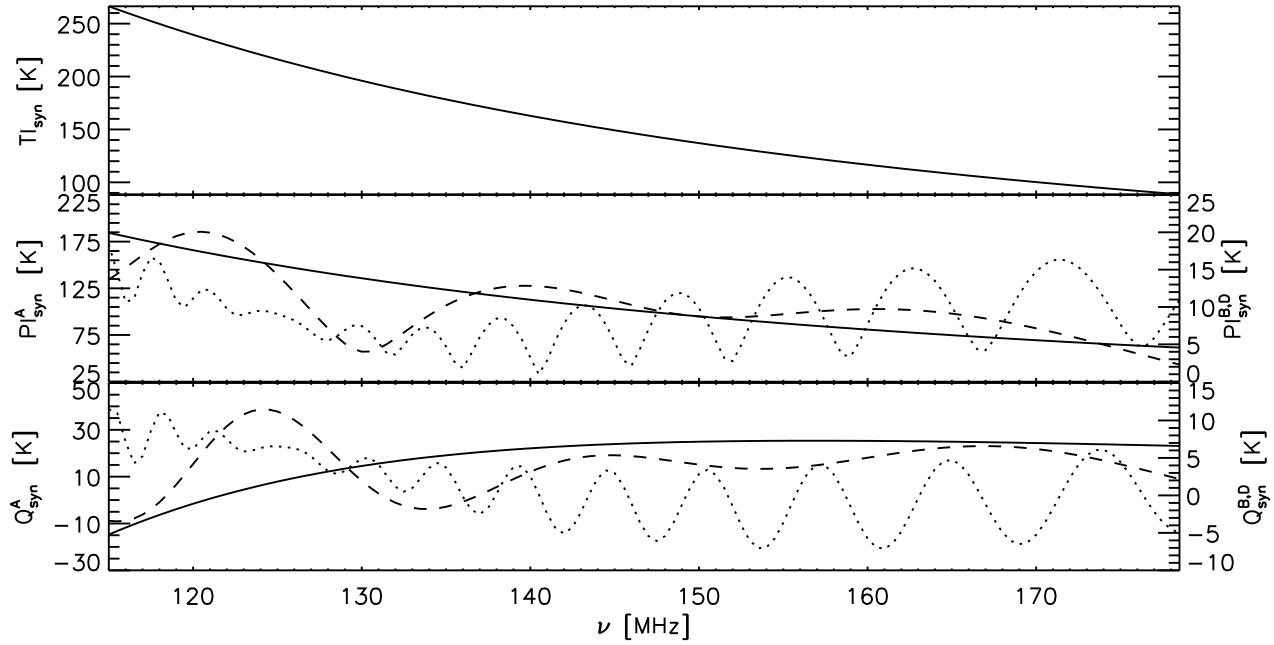

Figure 5. A random line through synchrotron total intensity (TI_{syn}) and polarized intensity (PI_{syn}, Q_{syn}) frequency data cubes. The *solid lines* are for the Galactic MODEL A, *dashed lines* for MODEL B and *dotted lines* for MODEL D. TI_{syn} is the same in all four models, while U_{syn} is not presented since it is similar to Q_{syn}. Note the polarized structures along the frequency direction. An improper polarization calibration of the instrument could cause a leakage of these structures to the total intensity and severely contaminate the EoR signal.

assume that $T_s \gg T_{\rm CMB}$, which is assumed in most of the current simulations.

The cosmological 21 cm maps (δT_b) are simulated using the BEARS algorithm (Thomas et al. 2009). BEARS is a fast algorithm to simulate the underlying cosmological 21 cm signal from the EoR. It is implemented using an N-body/SPH simulation in conjunction with a 1-D radiative transfer code under the assumption of spherical symmetry of the ionized bubbles. The basic steps of the algorithm are as follows: first, a catalogue of 1D ionization profiles of all atomic hydrogen and helium species and the temperature profile that surround the source is calculated for different types of ionizing sources with varying masses, luminosities at different redshifts. Subsequently, photon rates emanating from dark matter haloes, identified in the N-body simulation, are calculated semi–analytically. Finally, given the spectrum, luminosity and the density around the source, a spherical ionization bubble is embedded around the source, whose radial profile is selected from the catalogue as generated above. For more details we refer to Thomas et al. (2009).

For the purpose of this paper we use the δT_b data cube (2D slices along the frequency/redshift direction) of the cosmological 21 cm signal for the 'Stars' patchy reionization model (see Thomas et al. 2009). The data cube consists of 850 slices in the frequency range from 115 MHz to 200 MHz with 0.1 MHz step (corresponding to redshift between 6 and 11.5). Slices have a size of 100 h^{-1} comoving Mpc and are defined on a 512^2 grid. An example of a random line of sight through simulated 21 cm data cube, with angular and frequency resolution matching that of LOFAR, is shown in Fig. 8.

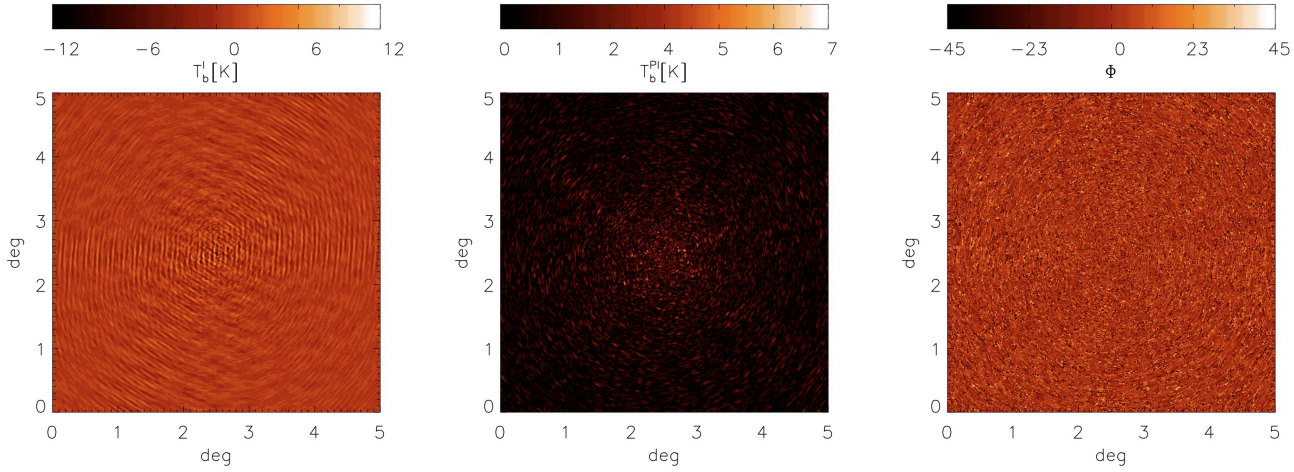

Figure 6. 'Dirty' maps of the simulated Galactic synchrotron emission (MODEL B) observed with the core stations of the LOFAR telescope. The total and polarized intensity maps are shown on the *first* and the *second panel*, while the polarization angle is presented on the *third panel*. The images are simulated at 138 MHz

.

6.2 Instrumental response

In order to produce the dirty maps of the diffuse emission, we calculate the 2D Fourier transform of the data for each correlation on a fine grid of 1.2 arcmin. We assume that there are 24 stations in the LOFAR array that are used for the observations. We then use a bilinear interpolation to estimate the values of the visibilities at the uvw points that correspond to the points sampled by the interferometer pairs of the core. This is done for 4hrs of synthesis, 10 sec integration and for the whole frequency range between 115 MHz and 180 MHz, using a step of 0.5 MHz. The above procedure is implemented as a parallel algorithm in the CHOPCHOP pipeline (see Labropoulos et al, *in preparation*). In order to sample the large structure of the foregrounds at scales between 5 and 10 degrees we need interferometer spacing between 6.5 and 13 meters. Thus the PSF acts as a high-pass spatial filter.

Figure 6 shows 'dirty' maps of the simulated Galactic synchrotron emission (MODEL B) observed with the core stations of the LOFAR telescope at 138 MHz. The total and polarized intensity maps are shown on the *first* and the *second panel*, while the polarization angle is presented on the *third panel*. Note that the large scale structures of the emission are missing as the smallest baseline length is approximately 50 m.

7 CALIBRATION ISSUES

One of the major challenges of the EoR experiments is the extraction of the EoR signal from the astrophysical foregrounds. The extraction is usually formed in total intensity along the frequency direction due to the following characteristics: the cosmological 21 cm signal is essentially unpolarized and fluctuates along the frequency direction (see Fig. 8), whereas the foregrounds are smooth along the frequency direction in total intensity and should only show fluctuations in polarized intensity (see Fig. 5, an example of the Galactic emission that is a dominant foreground component).

All current EoR radio interferometric arrays have an instrumentally polarized response, which needs to be calibrated. If the calibration is imperfect, some part of the polarized signal is transferred into a total intensity and vice versa (hereafter 'leakages'). As a result, the extraction of the EoR signal is more demanding.

Moreover, the polarized signal could have similar frequency fluctuations as the cosmological signal and as such could possibly severely contaminate it. Thus, to reliably detect the cosmological signal it is essential to minimize the 'leakages. We illustrate this thorough an example for the LOFAR telescope, but the problem is common to all current and planned EoR radio arrays.

The 'leakages' of the total and polarized signal are produced by two effects: the geometry of the LOFAR array and the cross-talk between the two dipoles in one LOFAR antenna. The cross-talk, a leakage in the electronics that can cause the power from one dipole to be detected with other, is small compared to the geometric effects and we will ignore it for the purpose of this paper. However, it will be taken into account in future work (Labropoulos et al, *in preparation*).

The geometry of the LOFAR telescope is such that the array antennae are fixed to the ground. Therefore, the sources are tracked only by beam-forming and not by steering the antennae mechanically towards the desired direction. This implies that, depending on the position of the source on the sky, a non-orthogonal (except in the zenith) projection of the two orthogonal dipoles is visible by the source. This projection further changes as the source is tracked over time. Thus, the observed Stokes brightness of the source, $\mathbf{S_{obs}}$, is given by (Carozzi & Woan 2009):

$$\mathbf{S}_{obs} = \mathbf{MS}, \tag{19}$$

where $\mathbf{M}$ is a Mueller matrix that quantifies the distortions of a true source brightness $\mathbf{S} = (I, Q, U, V)$ based on above geometry-projection effect. The Mueller matrix is defined as:

$$\mathbf{M} = \begin{pmatrix} \frac{1}{2}(1+n^2) & -\frac{m^2}{2} + \frac{(1+m^2)l^2}{2(1-m^2)} & -\frac{lmn}{1-m^2} & 0 \\ \frac{1}{2}(l^2-m^2) & 1 - \frac{m^2}{2} - \frac{(1+m^2)l^2}{2(1-m^2)} & \frac{lmn}{1-m^2} & 0 \\ -lm & -lm & n & 0 \\ 0 & 0 & 0 & n \end{pmatrix} \tag{20}$$

with the assumption of a coplanar array. Note that (l, m, n) are direction cosines and that the level of geometry-projection 'leakage' therefore varies across the map.

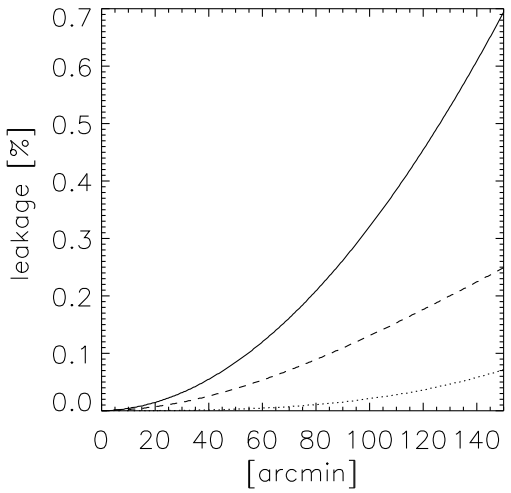

Figure 7. Simulated leakages for LOFAR telescope observing at 138 MHz an $5^\circ \times 5^\circ$ patch of the sky around the zenith. The obtained total and polarized intensity maps of Galactic emission (MODEL B) are used as a sky model and an instant imaging is assumed. Solid line presents the leakage of total intensity, and of polarized intensity is presented with dashed line (Stokes Q) and dotted line (Stokes U): see Eq. 20. The leakages are plotted as a function of distance from the center of the image along its diagonal.

Figure 7 shows calculated leakages for the LOFAR telescope observing at 138 MHz a $5^\circ \times 5^\circ$ patch of the sky around the zenith. For the sky model we use the total and polarized intensity maps of Galactic emission (model B). Further, an instant imaging is assumed, i.e. the sky is not tracked over time. The solid line presents the leakage of total intensity (Stokes I), the polarized signal is presented with the dashed line (Stokes Q) and the dotted line (Stokes U). The leakages are plotted as a function of distance from the center of the image along its diagonal. Note that the leakages are tiny around the center of the image, but they increase towards the edges.

The same calculation we repeat for an patch of a sky at 45° altitude. The leakages are now much larger, e.g. for the center of the image the leakage to the total intensity is around 2%, but can reach 20% towards the edges of the image. Once the tracking of the sources is taken into account, the calculation becomes even more complex. Detailed results on this issue will be addressed in a forthcoming paper (Labropoulos et al, in preparation).

Here we would like to point out that the 'leakages' caused by the geometry-projection effect are significant. Moreover, if these 'leakages' are not taken properly into account during the calibration of the instrument, the polarized Galactic emission could creep into total intensity signal and severely contaminate the EoR signal (see Fig. 8). In other words, the observing window for the EoR experiment should be in regions of the Galaxy that have very low polarized emission and calibration of the instrument should be preformed with such a precession that any remaining residuals of the polarized 'leakages' to the total intensity are much smaller than the EoR signal.

8 SUMMARY AND OUTLOOK

This paper presents Galactic foreground simulations used as templates for the LOFAR-EoR testing pipeline. The simulations provide maps of the Galactic free-free emission and the Galactic synchrotron emission both in total and polarized intensity. The maps are $10^\circ \times 10^\circ$ in size, with ~ 1 arcmin resolution and cover the frequency range between 115 and 180 MHz pertaining to the LOFAR-EoR experiment. The code however is flexible as can provide simulation over any scale with any spatial and frequency resolution.

The Galactic emission is calculated from a 3D distribution of cosmic ray and thermal electrons, and the Galactic magnetic field. The model assumes two magnetic field components: regular and random. The latter magnetic field and the thermal electron density are simulated as Gaussian random fields with power law power spectra. In addition, the spatial variations of the energy spectral index p of the cosmic ray electrons are introduced to mimic the observed fluctuations of the brightness temperature spectral index β. Note that all parameters of the simulation can be tuned to any desired value and this allows to explore the whole parameter space.

The total and polarized Galactic maps are obtained for four different models of Galactic emission (see Fig. 3 & 4). The first assumes that synchrotron and free-free emitters are spatially separated, such that thermal plasma acts as a "Faraday screen". The amplitude of the polarized emission is unchanged, while the polarization angles Faraday rotate. Other three simulation have regions where both types of emitters are mixed in different ways. The synchrotron emission is differentially Faraday rotated and depolarization occurs (see Table 2).

The main result of our simulations is that we are able to produce Galactic polarized synchrotron emission that is structured along the frequency direction (see Fig. 5) comparable to observations. The importance of this result comes from the fact that the planned EoR radio arrays have a polarized response and the extraction of the EoR signal from the foregrounds is usually performed along the frequency direction. Therefore, if the Galactic foreground is a smooth function (superposition of power laws) along the frequency in a total intensity and it fluctuates in polarized intensity. And the EoR signal is fluctuates along the frequency direction in total intensity, a calibration of the instrumental polarized response can transfer a fraction of the polarized signal into a total intensity. As a result, the leaked polarized emission can mimic the cosmological signal and make its extraction very difficult (see Fig. 8).

Finally we emphasize that the main aim of this paper has been to present the new Galactic emission model in total and polarized intensity that will be used as a foreground template for the LOFAR-EoR testing pipeline. Forthcoming papers will use the foreground simulations developed in this paper and in Jelić et al. (2008), together with simulations of the EoR signal (Thomas et al. 2009) and instrumental response (Labropoulos et al. 2009) to test all aspects of the LOFAR-EoR experiment and find the ultimate method for extraction of the cosmological 21 cm signal.

ACKNOWLEDGEMENT

We acknowledge discussion with the LOFAR-EoR key project members. As LOFAR members authors are partly funded by the European Union, European Regional Development Fund, and by 'Samenwerkingsverband Noord-Nederland', EZ/KOMPAS.

REFERENCES

Ali S. S., Bharadwaj S., Chengalur J. N., 2008, MNRAS, 385, 2166

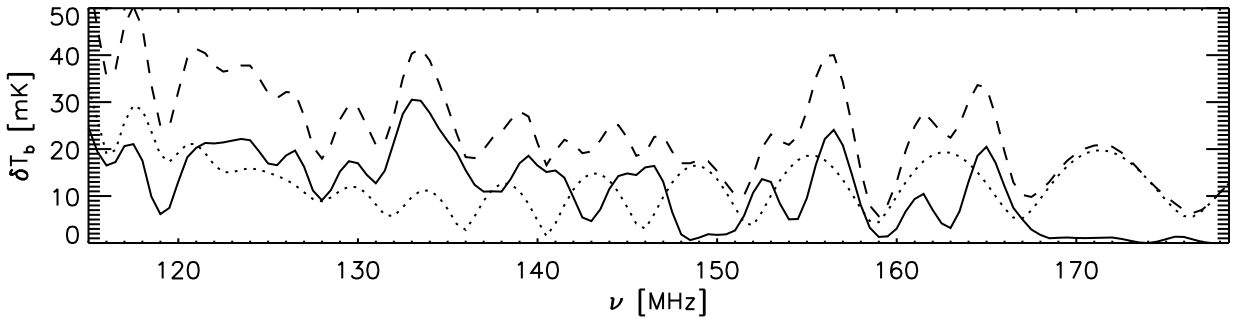

Figure 8. A random line of sight through a simulated 21 cm data cube for the 'Stars' patchy reionization history model (*solid line*). *Dotted line* shows the 'leakage' of the polarized Galactic emission to the total intensity and *dashed line* is a sum of the two. We assume 0.15% residual 'leakage' and we use model D as an example of the Galactic emission. The angular and frequency resolution of the data match that of the LOFAR telescope.

Beck R., Brandenburg A., Moss D., Shukurov A., Sokoloff D., 1996, ARA&A, 34, 155

Bennett C. L., Hill R. S., Hinshaw G., Nolta M. R., Odegard N., Page L., Spergel D. N., Weiland J. L., Wright E. L., Halpern M., Jarosik N., Kogut A., Limon M., Meyer S. S., Tucker G. S., Wollack E., 2003, ApJS, 148, 97

Berkhuijsen E. M., Mitra D., Mueller P., 2006, Astronomische Nachrichten, 327, 82

Bernardi G., Carretti E., Fabbri R., Sbarra C., Poppi S., Cortiglioni S., Jonas J. L., 2004, MNRAS, 351, 436

Bernardi G., de Bruyn A. G., Brentjens M. A., Ciardi B., Harker G., Jelić V., Koopmans L. V. E., Labropoulos P., Offringa A., Pandey V. N., Schaye J., Thomas R. M., Yatawatta S., Zaroubi S., 2009, A&A, 500, 965

Bowman J. D., Morales M. F., Hewitt J. N., 2009, ApJ, 695, 183

Brentjens M. A., de Bruyn A. G., 2005, A&A, 441, 1217

Carozzi T. D., Woan G., 2009, MNRAS, 395, 1558

Ciardi B., Madau P., 2003, ApJ, 596, 1

Cooray A., 2004, PhRvD, 70, 063509

Cordes J. M., Lazio T. J. W., 2002, ArXiv Astrophysics e-prints

de Bruyn A. G., Katgert P., Haverkorn M., Schnitzeler D. H. F. M., 2006, Astronomische Nachrichten, 327, 487

de Bruyn G., Miley G., Rengelink R., et al., 1998, WENSS. ASTRON

de Oliveira-Costa A., Tegmark M., Gaensler B. M., Jonas J., Landecker T. L., Reich P., 2008, MNRAS, 388, 247

Di Matteo T., Ciardi B., Miniati F., 2004, MNRAS, 355, 1053

Di Matteo T., Perna R., Abel T., Rees M. J., 2002, ApJ, 564, 576

Fan X., Strauss M. A., Becker R. H., White R. L., Gunn J. E., Knapp G. R., Richards G. T., Schneider D. P., Brinkmann J., Fukugita M., 2006, AJ, 132, 117

Field G., 1958, Procedings of the IRE, 132, 240

Field G. B., 1959, ApJ, 129, 536

Gaensler B. M., Madsen G. J., Chatterjee S., Mao S. A., 2008, Publications of the Astronomical Society of Australia, 25, 184

Gleser L., Nusser A., Benson A. J., 2008, MNRAS, 391, 383

Han J., Wielebinski R., 2002, Chinese Journal of Astronomy and Astrophysics, 2, 293

Harker G., Zaroubi S., Bernardi G., Brentjens M. A., de Bruyn A. G., Ciardi B., Jelić V., Koopmans L. V. E., Labropoulos P., Mellema G., Offringa A., Pandey V. N., Schaye J., Thomas R. M., Yatawatta S., 2009a, MNRAS, 397, 1138

Harker G. J. A., Zaroubi S., Thomas R. M., Jelić V., Labropoulos P., Mellema G., Iliev I. T., Bernardi G., Brentjens M. A., de Bruyn A. G., Ciardi B., Koopmans L. V. E., Pandey V. N., Pawlik A. H., Schaye J., Yatawatta S., 2009b, MNRAS, 393, 1449

Haslam C. G. T., Salter C. J., Stoffel H., Wilson W. E., 1982, A&AS, 47, 1

Haverkorn M., Katgert P., de Bruyn A. G., 2003, A&A, 403, 1045

Jelić V., Zaroubi S., Labropoulos P., Thomas R. M., Bernardi G., Brentjens M. A., de Bruyn A. G., Ciardi B., Harker G., Koopmans L. V. E., Pandey V. N., Schaye J., Yatawatta S., 2008, MNRAS, 389, 1319

Komatsu E., Dunkley J., Nolta M. R., Bennett C. L., Gold B., Hinshaw G., Jarosik N., Larson D., Limon M., Page L., Spergel D. N., Halpern M., Hill R. S., Kogut A., Meyer S. S., Tucker G. S., Weiland J. L., Wollack E., Wright E. L., 2009, ApJS, 180, 330

Labropoulos P., Koopmans L. V. E., Jelic V., Yatawatta S., Thomas R. M., Bernardi G., Brentjens M., de Bruyn G., Ciardi B., Harker G., Offringa A., Pandey V. N., Schaye J., Zaroubi S., 2009, ArXiv e-prints

Landecker T. L., Wielebinski R., 1970, Australian Journal of Physics Astrophysical Supplement, 16, 1

Morales M. F., Bowman J. D., Hewitt J. N., 2006, ApJ, 648, 767

Oh S. P., Mack K. J., 2003, MNRAS, 346, 871

Pacholczyk A. G., 1970, Radio astrophysics. Nonthermal processes in galactic and extragalactic sources. Freeman

Page L., Hinshaw G., Komatsu E., Nolta M. R., Spergel D. N., Bennett C. L., Barnes C., Bean R., Doré O., Dunkley J., Halpern M., Hill R. S., Jarosik N., Kogut A., Limon M., Meyer S. S., Odegard N., Peiris H. V., Tucker G. S., Verde L., Weiland J. L., Wollack E., Wright E. L., 2007, ApJS, 170, 335

Pen U.-L., Chang T.-C., Hirata C. M., Peterson J. B., Roy J., Gupta Y., Odegova J., Sigurdson K., 2009, MNRAS, 1240

Platania P., Bensadoun M., Bersanelli M., de Amici G., Kogut A., Levin S., Maino D., Smoot G. F., 1998, ApJ, 505, 473

Reich P., Reich W., 1986, A&AS, 63, 205

—, 1988, A&AS, 74, 7

Reich W., 2006, ArXiv Astrophysics e-prints

Reynolds R. J., 1990, in IAU Symposium, Vol. 139, The Galactic and Extragalactic Background Radiation, Bowyer S., Leinert C., eds., pp. 157–169

Rogers A. E. E., Bowman J. D., 2008, AJ, 136, 641

Rybicki G. B., Lightman A. P., 1986, Radiative Processes in Astrophysics. Wiley-VCH

Santos M. G., Cooray A., Knox L., 2005, ApJ, 625, 575

Schnitzler D., 2008, PhD thesis, Leiden Observatory, Leiden University, P.O. Box 9513, 2300 RA Leiden, The Netherlands

Shaver P. A., Windhorst R. A., Madau P., de Bruyn A. G., 1999,

A&A, 345, 380
Spergel D. N., Bean R., Doré O., Nolta M. R., Bennett C. L., Dunkley J., Hinshaw G., Jarosik N., Komatsu E., Page L., Peiris H. V., Verde L., Halpern M., Hill R. S., Kogut A., Limon M., Meyer S. S., Odegard N., Tucker G. S., Weiland J. L., Wollack E., Wright E. L., 2007, ApJS, 170, 377
Strong A. W., Moskalenko I. V., Reimer O., Digel S., Diehl R., 2004, A&A, 422, L47
Sun X. H., Reich W., 2009, ArXiv e-prints
Sun X. H., Reich W., Waelkens A., Enßlin T. A., 2008, A&A, 477, 573
Thomas R. M., Zaroubi S., Ciardi B., Pawlik A. H., Labropoulos P., Jelić V., Bernardi G., Brentjens M. A., de Bruyn A. G., Harker G. J. A., Koopmans L. V. E., Mellema G., Pandey V. N., Schaye J., Yatawatta S., 2009, MNRAS, 393, 32
Waelkens A., Jaffe T., Reinecke M., Kitaura F. S., Enßlin T. A., 2009, A&A, 495, 697
Wang X., Tegmark M., Santos M. G., Knox L., 2006, ApJ, 650, 529
Webber W. R., Simpson G. A., Cane H. V., 1980, ApJ, 236, 448
Wieringa M. H., de Bruyn A. G., Jansen D., Brouw W. N., Katgert P., 1993, A&A, 268, 215
Wilson T. L., Rohlfs K., Hüttemeister S., 2009, Tools of Radio Astronomy. Springer

This paper has been typeset from a TEX/ LATEX file prepared by the author.